A Simplified Approach to Modeling Exhaust System Emissions: SIMTWC

Paul M. Laing, Michael D. Shane, Seha Son, Andrew A. Adamczyk and Peter Li
Ford Motor Co.

ABSTRACT

The optimized design of an exhaust emission system in terms of performance, cost, packaging, and engine control strategy will be a key part of competitively meeting future more stringent emission standards. Extensive use of vehicle experiments to evaluate design system tradeoffs is far too time consuming and expensive. Imperative to successfully meeting the challenges of future emission regulations and cost constraints is the development of an exhaust system simulation model which offers the ability to sort through major design alternatives quickly while assisting in the interpretation of experimental data.

Previously, detailed catalyst models have been developed which require the specification of intricate kinetic mechanisms to determine overall catalyst performance. While yielding extremely valuable results, these models use complex numerical algorithms to solve multiple partial differential equations which are time consuming and occasionally numerically unstable. Furthermore, keeping these kinetic data updated with improvements in catalyst formulations is also a very time consuming process. To resolve these issues, a simple model (SIMTWC, which stands for SIMple Three Way Catalyst) to predict tailpipe exhaust emissions has been developed by combining fundamental conservation expressions for mass and energy with a first order oxygen storage model and an empirical data base of steady-state catalyst performance obtained during engine dynamometer assessments, thus eliminating the need to specify the detailed kinetic mechanisms. Advantages of SIMTWC over more complicated techniques are computational expedience and robustness with comparable accuracy. Updates to SIMTWC as catalyst formulations change are also accomplished in a timelier manner.

This paper describes the mathematical formulation of SIMTWC, solution technique, input data requirements, and provides a comparison of model results with vehicle experiments.

INTRODUCTION

Historically, models of emission system performance required the specification of detailed kinetic mechanisms through the catalyst element to predict their performance [see, Oh,S. (1980), Otto,N. (1980), Montreuil, et al. (1992), Koltsakis, et al. (1997)]. During a calculation, these models specify and solve a set of partial differential equations to calculate the temperature and species evolution within the catalyst. The numerical algorithms are complex and time consuming. Herein, we take a simpler approach while retaining many of the key features of the more complex models. A first principle transient energy balance model is used to account for the substrate heat transfer dynamics, but we replace the integration of the species conservation equations with a steady state map of catalyst performance obtained during assessment on an engine dynamometer or reactor. Because of this feature, the numerical integration is reduced to the solution of the transient energy equations and an integration to specify the time-dependent O_2 storage over the catalyst [Gandhi, H.S. (1976)]. This results in a more robust calculation and one in which a calculation can be performed rapidly with accuracy similar to that produced by the more complex models.

The overall objectives of this modeling approach are:

1. To allow rapid and early design assessments of new concepts proposed for production exhaust/emission systems;

2. To support the interpretation of experimental data and to serve as a means of establishing a corporate memory of lessons learned during experimentation; and

3. To allow the easy integration of component models into larger system assessment models.

Here, a "SIMPLE WORKING MODEL" approach is used in the development of SIMTWC. The model is simple enough in formulation to allow rapid calculation but retains sufficient detail so that the results are meaningful for emission system development.

1

The basic assumptions that allow this simpler approach are:

1. The steady state chemistry on the catalyst is fast when compared to the heat transfer dynamics and the O_2 storage chemistry. This quasi-steady state assumption implies that the reaction rates of relevant emission species (HC, CO, and NOx) can be represented at any instant by an experimental steady-state performance map generated over a variety of key conditions (viz., substrate temperature, space velocity, air fuel ratio, and inlet gas species concentrations); and

2. Oxygen storage kinetics on the catalyst can be represented as the filling or emptying of surface storage sites in correspondence with a first order kinetic mechanism. Since this feature happens over time scales that are typically longer than those associated with the steady state kinetics, a site balance expression is integrated in time as well.

Each catalyst of a given precious metal (PM) formulation/loading and aging history will have a unique performance characteristic (or "potency") represented by its own set of mapping experiments. The number of experiments needed to characterize a particular catalyst is small enough to permit the rapid generation of new maps as catalyst formulations change/improve.

In the SIMTWC representation, the model allows the determination of simple heat transfer in a pipe element ahead of the catalyst and the determination of temperature and species in a catalyst element. This combination of elements acts as a fundamental building block to allow the assessment of a complete exhaust system. Generally, these elements are combined in series/parallel combinations that represent the action in a complete vehicle exhaust system. To use the model, precise exhaust system geometry, feedgas temperature, mass flow rate, A/F ratio, and species concentration are needed for each second during a typical driving cycle.

MATHEMATICAL FORMULATION

THE PIPE ELEMENT – The effects of the thermal mass and heat transfer characteristics along the exhaust system piping are extremely important in the determination of the exhaust system temperature. This is especially true during cold start of the vehicle when the entire system is warmed from ambient conditions to operational temperature. They are therefore important to catalyst light off and critical to meeting governmental emissions regulations, such as California LEV II or European Stage IV. The effects of thermal mass and convective heat transfer (between the gas and wall, and between the wall and atmosphere, plus thermal conduction along the wall) on the gas and wall temperature are determined using the conservation of energy for the gas phase (Eq. 1) and the surface (Eq. 2). (Note: all definitions of variables, units, and many physical properties are included in the nomenclature section).

$$\dot{m}_g Cp_g \frac{\partial T_g}{\partial z} = -h_I P_{I_{pipe}} \left(T_g - T_w \right) \tag{1}$$

$$A_{w_{pipe}} \rho_w Cp_w \frac{\partial T_w}{\partial t} = \lambda_w A_{w_{pipe}} \frac{\partial^2 T_w}{\partial z^2}$$
$$+ h_I P_{I_{pipe}} \left(T_g - T_w \right)$$
$$- h_O P_{O_{pipe}} \left(T_w - T_{amb} \right) \tag{2}$$

where: T_g, T_w, and T_{amb} are the gas, the wall and ambient temperatures, respectively. The thermal conductivity of the pipe wall is λ_w, and $A_{w_{pipe}}$ is its cross-sectional area; h_I and h_O are the internal and external heat transfer coefficients, respectively. Heat transfer between the exhaust gas and the inside pipe wall occurs under turbulent flow conditions and h_I is determined from:

$$h_I = \frac{Nu_I \cdot \lambda_g}{D_{I_{pipe}}} \cdot a_I \tag{3}$$

$$Nu_{I(turbulent)} = 0.023 \cdot Re^{0.8} \cdot Pr^{0.3} \left(\frac{\mu_g(T_g)}{\mu_g(T_f)} \right)^{0.14} \tag{4}$$

$$Re = \frac{4\dot{m}_g}{\pi D_{I_{pipe}} \mu_g(T_g)} \tag{5}$$

$$Pr = \frac{\mu_g(T_g) \cdot Cp_g}{\lambda_g} \tag{6}$$

$$A_{w_{pipe}} = \frac{\pi}{4} \cdot \left(D_{O_{pipe}}^2 - D_{I_{pipe}}^2 \right) \tag{7}$$

where: a_I is an augmentation factor that can be used to account for increased internal heat transfer due to pulsating exhaust flow and/or pipe bends. T_f is the film temperature which equals the average of T_g and T_w. $D_{I_{pipe}}$ and $D_{O_{pipe}}$ are the pipe inside and outside diameters. The outside heat transfer mode in the SIMTWC calculation is approximated by an equation for free convection over a horizontal cylinder, and the corresponding heat transfer coefficient is:

$$h_O = \frac{Nu_O \cdot \lambda_{air}}{D_{O_{pipe}}} \cdot a_O \tag{8}$$

where:

2

$$Nu_O = 0.53 \cdot \left(Gr \cdot \Pr\right)^{0.25} \tag{9}$$

$$Gr \equiv \left(\frac{g \cdot \beta \cdot (T_w - T_{amb}) \cdot D_{O_{pipe}}^3}{\mu_g^2(T_{amb})}\right) \tag{10}$$

a_O is an augmentation factor to account for a small degree of forced convection due to air movement past the outside of the pipe, g is the gravitational constant, and β is the gas expansion coefficient and equals the reciprocal of absolute gas temperature.

Boundary and initial conditions are necessary for complete problem definition and are specified as:

$$\frac{\partial T_{w_{(z=0)}}^{t \geq 0}}{\partial z} = \frac{\partial T_{w_{(z=L_{pipe})}}^{t \geq 0}}{\partial z} = 0 \tag{11}$$

$$T_{g_{(z=0)}}^t = T_{g,inlet}(t) \tag{12}$$

$$T_{w_z}^{t=0} = T_w^0(z) \tag{13}$$

where the first boundary condition (Eq. 11) indicates that no heat is transferred at the ends of the system, and the initial condition (Eq. 13) can be used to specify an initial longitudinal temperature distribution along the wall.

The above equations are used to account for the heat losses along the exhaust piping in the system. Currently, this pipe model does not include any additional chemical heat generation that may be generated in the exhaust manifold near the engine as a result of gas phase chemistry under very hot conditions. However, most simulation results are not affected by this factor because under typical drive cycle conditions, gas phase reaction is minimal, and the starting point for most simulations is downstream of the manifold flange beyond any significant level of reaction.

THE CATALYST ELEMENT – We start our formulation for the catalyst with the generalized conservation equations as seen in [Otto (1980), Li, Adamczyk and Pakko (1996) or Oh (1980)] and then simplify them into the form used in the integration of the SIMTWC model, remembering that SIMTWC is specifically designed to quickly and robustly analyze exhaust/ emissions systems. The following expressions specify the conservation of mass and energy in the gas phase and on the surface of the catalyst. They also represent the convective transport of species and energy to and from the surface as well as conduction along the surface, as shown in Figure 1. They also include chemical mechanisms to represent O_2 storage on the catalyst surface and steady state surface chemistry. In the SIMTWC model, a database map of catalyst performance is used as the final representation of the steady state kinetics. This is done to reduce the total number of conservation equations to allow fast integra-

tion of the equation set. It is also done to easily incorporate mapping data of catalyst performance.
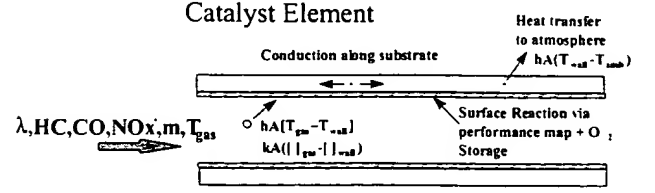

Figure 1. Schematic of catalyst flow element

Conservation of Energy, Species and Mass and Initial and Boundary Conditions: Gas & Surface

$$\varepsilon \rho_g Cp_g \frac{\partial T_g}{\partial t} = -\varepsilon v_g \rho_g Cp_g \frac{\partial T_g}{\partial z} - h_t Ga(T_g - T_w) \tag{14}$$

$$(1-\varepsilon)\rho_w Cp_w \frac{\partial T_w}{\partial t} = \lambda_w (1-\varepsilon)\frac{\partial^2 T_w}{\partial z^2} + h_t Ga(T_g - T_w) - h_O S_{ext}(T_w - T_{amb}) + Ga \sum_{k=1}^{N_{react}} R_k(T_w, C_w^1, ..., C_w^{N_{species}}) \cdot \Delta H_k \tag{15}$$

$$\varepsilon \frac{\partial C_g^i}{\partial t} = -\varepsilon v_g \frac{\partial C_g^i}{\partial z} - k_m^i Ga(C_g^i - C_w^i) \quad (i = 1, 2, ..., N_{species}) \tag{16}$$

$$(1-\varepsilon)\frac{\partial C_w^i}{\partial t} = k_m^i Ga(C_g^i - C_w^i) - Ga \cdot R^i(T_w, C_w^1, ..., C_w^{N_{species}}) \quad (i = 1, 2, ..., N_{species}) \tag{17}$$

$$(1-\varepsilon)\frac{\partial C_{O_2,store}^i}{\partial t} = -Ga \cdot R^i(T_w, C_w^1, ..., C_w^{N_{species}}) \quad (i = O_2^{Ox}, O_2^{Red}) \tag{18}$$

$$\dot{m}_g = \rho_g \dot{V}_g = \rho_g \varepsilon v_g A_{face} \tag{19}$$

where ε is the void volume fraction of the monolith as calculated from its geometry, v_g is the gas velocity within a catalyst channel, and A_{face} is the total frontal area of the catalyst. In the catalyst, the heat transfer between exhaust gas and catalyst wall is based on a laminar flow Reynolds number (based on the flow through a single catalyst channel using Eq. 20).

3

$$\text{Re} = \frac{\dot{m}_g / (CD \cdot A_{face})}{D_{l_{cat}} \mu_g (T_g)}$$

(20)

where CD is the cell density, $D_{l_{cat}}$ is the hydraulic diameter of a single channel in the monolith and is related to monolith cell density, wall thickness and cell shape according to the equation shown in the Nomenclature Section. The corresponding Nusselt number with appropriate entrance effect enhancement is:

$$Nu_{l \text{ (laminar)}} = 2.709 \cdot \left(\text{Re} \cdot \text{Pr} \cdot \frac{D_{l_{cat}}}{z} \right)^{0.179}$$

(21)

where z is the longitudinal distance from entrance of the monolith.

To solve this equation set, one must specify several initial conditions for the exhaust system and one must specify gas inlet temperature, flow rate, and species concentrations on a second-by-second basis during the specific drive cycle under consideration. These conditions are specified as:

$$T_{g_z}^{t=0} = T_{w_z}^{t=0} = T_z^0$$

(22)

$$\dot{m}_g (0 \leq \bar{z} \leq 1; t) = \dot{m}_{g.inlet}(t)$$

(23)

$$T_{g_{(\bar{z}=0)}}^t = T_{g,inlet}(t)$$

(24)

$$\frac{\partial T_{w_{(\bar{z}=0)}}^t}{\partial \bar{z}} = \frac{\partial T_{w_{(\bar{z}=1)}}^t}{\partial \bar{z}} = 0$$

(25)

$$C_g^i (0 \leq \bar{z} \leq 1; t = 0) = C_w^i (0 \leq \bar{z} \leq 1; t = 0)$$

$$= C_0^i$$

(26)

$$C_g^i (\bar{z} = 0; t) = C_{g,inlet}^i(t)$$

(27)

where $\bar{z} = z / L_{cat}$ = normalized length along the catalyst.

The Simplified Catalyst Model – We now proceed to reduce the equation set from this generalized form to the simplified form used in SIMTWC. As a first simplification to this equation set, the transient terms ($\partial / \partial t$) in the gas phase energy (Eq. 14), the gas phase species concentration (Eq. 16), and the steady state surface species conservation (Eq. 17) expressions are neglected as in previous analysis [see Otto, (1980); Oh, (1980); Li, Adamczyk and Pakko, (1996); Koltsakis, (1997)] where they were shown to be small in comparison with the remaining terms. In addition, the definition of the void volume fraction, ε, and the geometric properties of a monolithic cell are incorporated to yield:

$$\dot{m}_g Cp_g \frac{\partial T_g}{\partial z} = -h_l P_{l_{cat}} (T_g - T_w)$$

(28)

$$A_{w_{cat}} \rho_w Cp_w \frac{\partial T_w}{\partial t} = \lambda_w A_{w_{cat}} \frac{\partial^2 T_w}{\partial z^2} + h_l P_{l_{cat}} (T_g - T_w)$$

$$- h_O P_{O_{cat}} (T_w - T_{amb})$$

$$+ P_{l_{cat}} \sum_{k=1}^{N_{react}} R_k (T_w, C_w, ..., C_w^{N_{species}}) \cdot \Delta H_k$$

(29)

$$\dot{m}_g \frac{\partial C_g^i}{\partial z} = -k_m^i P_{l_{cat}} \rho_g (C_g^i - C_w^i)$$

$$(i = 1, 2, ..., N_{species})$$

(30)

$$k_m^i (C_g^i - C_w^i) = R^i (T_w, C_w^1, ..., C_w^{N_{species}})$$

$$(i = 1, 2, ..., N_{species})$$

(31)

$$\frac{\partial C_{O_2,store}^i}{\partial t} = -\frac{P_{l_{cat}} \cdot R^i (T_w, C_w^1, ..., C_w^{N_{species}})}{A_{w_{cat}}}$$

$$(i = O_2^{Ox}, O_2^{Red})$$

(32)

where:

$$\frac{A_{w_{cat}}}{A_{face}} = (1 - \varepsilon); \quad S_{ext} = \frac{P_{O_{cat}}}{A_{face}}; \quad Ga = \frac{P_{l_{cat}}}{A_{face}}$$

(33)

To allow rapid, robust calculation, we assume that the mass transfer rate is fast when compared to the surface reaction rate at low to mid operating temperatures; and it is augmented at high operating temperatures in the final model to accommodate conditions where the surface reaction is very fast and the overall catalyst conversion is limited by the mass transfer rate. Thus,

$$C_w^i \approx C_g^i$$

(34)

and the gas phase species (Eq. 30) and surface species (Eq. 31) balance equations combine to yield:

$$\frac{\partial C_w^i}{\partial z} = -\frac{P_{l_{cat}}}{V_g} \cdot R^i (T_w, C_w^1, ..., C_w^{N_{species}})$$

$$(i = 1, 2, ..., N_{species})$$

(35)

In order to solve Eq. 35 explicitly, one would need a detailed function for the reaction rate expression, R^i, complete with rate constants, and reaction orders. However, for simplicity and speed, we solve the species equations in a global sense by using mapping data to specify the overall steady state conversion efficiency and a transient O_2 storage integration; O_2 storage will be discussed later. The catalyst performance map generated either in a reactor or on an engine dynamometer yields the overall change in species concentration across the total length of the catalyst at discrete temperatures and flow rates for

a particular catalyst geometry and formulation providing solutions to Eq. 35, but only for a limited number of conditions. (It would be too time consuming and expensive to generate a catalyst map which would cover all possible operating conditions). We extrapolate the utility of the catalyst performance map by examining how the overall conversion is distributed locally along the catalyst length when a simplified reaction mechanism is considered to develop a scaling relationship between the catalyst map and the conditions being modeled.

For example, suppose the reaction rate expression for each species i has the following simplified form:

$$R^i(T_w, C_w^1, ..., C_w^{N_{species}}) = r_{T_w}(C_w^i)^{n_{order}}$$
(36)

where r_{T_w} is the reaction rate constant at T_w and n_{order} is the reaction rate order. Substituting this expression into Eq. 35 and rearranging yields the following expression:

$$-\frac{\partial C_w^i}{(C_w^i)^{n_{order}}} = \frac{P_{l_{cat}}}{\dot{V}_g} \cdot r_{T_w} \cdot \partial z$$
(37)

The numerical solution technique (presented later in this report) relies on the breakdown of the catalyst into a number of longitudinal computational elements. Consequently, it will be necessary to determine how the surface concentration changes on a cell by cell basis. This is obtained by integrating Eq. 37 over a the length of a single computational element to yield:

$$C_{w_j}^i = \left[(C_{w_{j-1}}^i)^{(1-n_{order})} + \frac{P_{l_{cat}} \cdot r_{T_w} \cdot \Delta z_j}{\dot{V}_g \cdot (n_{order}-1)}\right]^{\frac{1}{(1-n_{order})}}$$
$$for \ n_{order} \neq 1, \ or$$
(38a)

$$C_{w_j}^i = C_{w_{j-1}}^i \cdot \exp\left(\frac{P_{l_{cat}}}{\dot{V}_g} \cdot r_{T_w} \cdot \Delta z_j\right)$$
$$for \ n_{order} = 1$$
(38b)

where Δz_j is the length of an individual computational cell at the jth location along the substrate, and $C_{w_j}^i$ is the concentration of species i exiting cell j.

Using Eq. 38 together with the definition of a local conversion efficiency, η_j^i, at the jth location along the substrate for species i, gives:

$$\eta_j^i \equiv \frac{C_{w_{j-1}}^i - C_{w_j}^i}{C_{w_{j-1}}^i} = 1.0 - \exp\left(\frac{P_{l_{cat}}}{\dot{V}_g} \cdot r_{T_w} \cdot \Delta z_j\right)$$
$$for \ n_{order} = 1, or$$
(39a)

$$\eta_j^i =$$

$$1.0 - \frac{\left[(C_{w_{j-1}}^i)^{(1-n_{order})} + \frac{P_{l_{cat}} \cdot r_{T_w} \cdot \Delta z_j}{\dot{V}_g \cdot (n_{order}-1)}\right]^{\frac{1}{(1-n_{order})}}}{C_{w_{j-1}}^i}$$
$$for \ n_{order} \neq 1$$
(39b)

These expressions for local catalyst efficiency are related to the overall catalyst efficiency provided by the catalyst map, η_{cat}^i, via the relationship shown in Eq. 40.

$$\eta_{cat}^i = \frac{C_{w_0}^i - C_{w_{Ncell}}^i}{C_{w_0}^i} = \frac{C_{w_{inlet}}^i - C_{w_{outlet}}^i}{C_{w_{inlet}}^i}$$

$$= 1.0 - \prod_{j=1}^{N_{cell}}(1-\eta_j^i)$$
(40)

Note that in the case of $n_{order} = 1$, Eq. 39a yields a local conversion efficiency that is independent of inlet concentration and will be uniform along the entire active portion of the substrate when uniform longitudinal computational cell spacing is used (i.e., $\Delta z_j = \Delta z = L_{cat}/N_{cell}$ for all j). For this special case, we define a uniform local efficiency as:

$$\eta_{j(uniform)}^i \equiv \frac{C_{w_j}^i - C_{w_{j+1}}^i}{C_{w_j}^i}$$

$$= 1.0 - \exp\left(\frac{P_{l_{cat}}}{\dot{V}_g} \cdot r_{T_w} \cdot \frac{L_{cat}}{N_{cell}}\right)$$
(41)

and rearrange Eq. 40 to give:

$$\eta_{j(uniform)}^i = 1 - (1 - \eta_{cat}^i)^{1/N_{cell}}$$
(42)

For a catalyst monolith with a square cell cross-section, Eq. 41 can be expressed as:

$$\eta_{j(uniform)}^i = 1.0 -$$

$$\exp\left(\frac{4 \cdot \sqrt{CD} \cdot (1 - W_t\sqrt{CD}) \cdot A_{face}}{\dot{V}_g} \cdot r_{T_w} \cdot \frac{L_{cat}}{N_{cell}}\right)$$
(43)

and the importance of the term in the exponential is that it gives the correct scaling relationship to extend our engine mapping data to catalysts of other geometries-- other cell densities and wall thickness, differing space velocity and differing volume. This allows us to replace the detailed species conservation kinetic expression with a concise catalyst performance map.

One can also distribute the overall catalyst conversion efficiency for each species to each calculation node along the length of the catalyst by solving for $\eta^i_{j(uniform)}$ and thereby estimate the energy release and species distribution along the substrate. In general, η^i_j is a function of many variables. Here, we have chosen one functional dependence which corresponds to the fast mass transfer assumption where the overall conversion is controlled by a simple chemical reaction mechanism which in practice has produced results which compare favorably with experimental data obtained during typical emission cycle conditions.

One can correlate other dependencies for special circumstances such as high space velocity conditions, to simulate an aging effect, or to mimic other unique features which occur during experimentation that are not well represented by the above simplification. SIMTWC is written in a manner in which these can be easily integrated.

With the above simplifications of fast mass transfer, local uniformity of conversion efficiency and quasi steady kinetics, the equation set reduces to

$$\dot{m}_g Cp_g \frac{\partial T_g}{\partial z} = -h_l P_{l_{cat}} (T_g - T_w) \tag{44}$$

$$A_{w_{cat}} \rho_w Cp_w \frac{\partial T_w}{\partial t} = \lambda_w A_{w_{cat}} \frac{\partial^2 T_w}{\partial z^2} + h_l P_{l_{cat}} (T_g - T_w)$$
$$- h_O P_{O_{cat}} (T_w - T_{amb}) + \dot{Q}_{chem} \tag{45}$$

$$\frac{\partial C^i_{O_2 store}}{\partial t} = -\frac{P_{l_{cat}} \cdot R^i (T_w, C^1_w, ..., C^{N_{species}}_w)}{A_{w_{cat}}}$$
$$= -\text{Constant} \cdot C^i_{O_2 store} \cdot fn(\overline{T}_w)$$
$$(i = O_2^{Ox}, O_2^{Red}) \tag{46}$$

where we utilize our estimate of local efficiency to distribute the exothermic chemical energy release discretely along the catalyst according to:

$$\dot{Q}_{chem,j} = \frac{N_{cell(active)}}{L_{cat(active)}} \sum_i^{Nred} \left(\eta^i_{j(uniform)} \right) C^i_g V_g (\Delta H_i)$$
$$(i = HC, CO, \& H_2) \tag{47}$$

$$\eta^i_{j(uniform)} = \left\{ 1 - \left(1 - \eta^i_{cat} \right)^{1/N_{cell(active)}} \right\} \tag{48}$$

$$\overline{T}_w = \sum_{j=1}^{N_{cell(active)}} T_{w_j} / N_{cell(active)} \tag{49}$$

where $\dot{Q}_{chem, j}$ is the exothermic heat released per "active" computational cell j (a computational cell is considered "active" if it is above a specified light-off temperature); $L_{cat(active)}$ is the length of catalyst that is "active"; $N_{cell(active)}$ is the number of active computational cells assuming uniform spacing; N_{red} is the number of reductants in the calculation; and $\overline{T}_w$ is the average surface temperature of the active cells. In SIMTWC, CO and H_2 are considered as one species where $C^{H_2}_g = \frac{1}{3} \cdot C^{CO}_g$ for gasoline [see Montreuil, Adamczyk, and Williams (1992) for a detailed discussion of why this is appropriate], and all HC are grouped as one species. In addition, to determine a total oxidant level, NOx is lumped together with oxygen (with one mole of NOx equivalent to ½ mole O_2). Thus, the energy liberated by reaction with O_2 is considered similar to that with NOx. Further, $C_{O2,store}$ refers to two surface species, -- an oxidized site and a reduced site. They are related through a site conservation equation specified as

$$C^{O_2^{Ox}}_{O_2 store} + C^{O_2^{Red}}_{O_2 store} = C^{Tot}_{O_2 store} \tag{50}$$

This equation set is solved using the initial and boundary conditions shown earlier (Eqs. 22 – 27) that specify gas inlet temperature, flow rate, and species concentrations on a second-by-second basis during the specific drive cycle under consideration.

The Oxygen Storage Model – As mentioned earlier, the oxygen storage mechanism in SIMTWC catalyst element is a transient phenomenon that removes oxygen from a lean exhaust gas stream and stores it on the surface of the catalyst. When the exhaust gas is rich relative to stoichiometry, the oxygen storage mechanism releases the oxygen stored on the catalyst surface to react with the reductants (CO and HCs) from the exhaust gas. The amount of oxygen that may be stored in the catalyst is called the total oxygen storage capacity and is a function of the amount of oxidizable material (e.g., ceria) in the washcoat of the catalyst. As the catalyst ages, the total oxygen storage capacity is reduced and the overall catalyst conversion efficiency generally declines with this reduction.

In this model implementation, the rate at which the oxygen is stored and released is a function of the exhaust mass flow rate, the exhaust air-fuel ratio, the catalyst temperature, the oxygen diffusion between the gas and surface, the oxygen storage/release reaction rates on the surface of the catalyst, the oxygen storage capacity, and the amount of oxygen already stored on the catalyst surface. As seen above, the oxygen storage model is a first order model that accounts for these factors. Here, the

exhaust gas oxygen excess or deficiency relative to stoichiometry, O_{2xcess}, expressed as a mole fraction, is given by

$$O_{2xcess} = \frac{(\lambda - 1)}{\left(\dfrac{y/4}{1 + y/4} + 4.76 \cdot \lambda \right)}$$

(51)

where y is the hydrogen-to-carbon ratio of the fuel, and λ is the stoichiometrically normalized air-to-fuel ratio of the exhaust gas. A positive O_{2xcess} $(\lambda > 1)$ indicates an excess of oxygen in the exhaust gas free stream while a negative O_{2xcess} $(\lambda > 1)$ indicates a deficiency of oxygen.

The normalized molar flow rate of excess/deficient oxygen into the catalyst, $\dot{m}_{xcess}$, is given by

$$\dot{m}_{xcess} = \frac{O_{2xcess} \cdot \dot{m}_{exh}}{O_{2,cap}}$$

(52)

where $\dot{m}_{exh}$ is the exhaust molar flow rate and $O_{2,cap}$ is the total oxygen storage capacity of the catalyst in moles/Kg of catalyst. Using

$$\frac{\partial C^i_{O_2 store}}{\partial t} = -\text{Constant} \cdot fn(\overline{T}_w) \cdot C^i_{O_2 store}$$

(53)

for each site species and the total O_2 storage site conservation (Eq. 50) as the species conservation equation which describes O_2 storage site action and defining

$$\chi_{O_2 store} = \frac{C^i_{O_2 store}}{O_{2,cap}}$$

(54)

Then the overall rate of oxygen storage/release is given by

$$\frac{\partial \chi_{O_2 store}}{\partial t} = k_i \cdot \dot{m}_{xcess} \cdot \chi_{O_2 store}$$

$$(i = store \,\&\, i = release)$$

(55)

where k_i is a lumped parameter that includes the effects of oxygen diffusion from the gas to the catalyst substrate and the oxygen storage or adsorption/reaction (i=store) and release or desorption/reaction (i=release) rates; and $\chi_{O_2 store}$ is the fractional filling of the oxygen storage capacity (or oxygen bucket), $0 \le \chi_{O_2 store} \le 1$. When there

is a deficiency of oxygen $(\lambda > 1)$, the rate of change of $\chi_{O_2 store}$ is:

$$\frac{\partial}{\partial t} \chi_{O_2 store} = k_{release} \cdot \chi_{O_2 store}$$

(56)

Thus, when the oxygen storage sites are nearly full $(\chi_{O_2 store} \approx 1)$, the oxygen release rate is near its maximum. Conversely, when the oxygen storage sites are nearly empty $(\chi_{O_2 store} \approx 0)$, the oxygen release rate is near zero. Furthermore, when there is an excess of oxygen $(\lambda > 1)$, the rate of change of (1- $\chi_{O_2 store}$) is proportional to (1 - $\chi_{O_2 store}$),

$$\frac{\partial}{\partial t} \left(1 - \chi_{O_2 store} \right) = -k_{store} \cdot \left(1 - \chi_{O_2 store} \right)$$

(57)

or,

$$\frac{\partial}{\partial t} \chi_{O_2 store} = k_{store} \cdot \left(1 - \chi_{O_2 store} \right)$$

(58)

Thus, when the oxygen storage is nearly full, the oxygen storage rate approaches zero. When the oxygen storage is nearly empty, the oxygen storage rate is near its maximum.

The effective relative air-fuel ratio, λ_{cat}, within the catalyst after the release or storage of oxygen remains to be calculated. The mole fraction of oxygen adsorbed or desorbed by the catalyst in a time interval dt, $O_{2,ads}$, is given by

$$O_{2,ads} = \frac{\displaystyle\int_t^{t+dt} \left(\frac{d}{dt} \chi_{O_2 store} \right) \cdot dt}{\displaystyle\int_t^{t+dt} \dot{m}_{exh} \cdot dt}$$

(59)

If $\left| O_{2,ads} \right| > \left| O_{2xcess} \right|$ then $O_{2,ads} = O_{2xcess}$. When $O_{2,ads} > 0$, oxygen is stored by the catalyst and λ_{cat} becomes richer. Conversely, when $O_{2,ads} < 0$, oxygen is released from storage and the λ_{cat} becomes leaner. In both cases, λ_{cat} moves toward the stoichiometric value of 1. The effective λ_{cat} is given by

$$\lambda_{cat} = \frac{\left(\dfrac{y/4}{1+y/4} \cdot \left(O_{2xcess} - O_{2,ads} \right) + 1 \right)}{\left(1 - 4.76 \cdot \left(O_{2xcess} - O_{2,ads} \right) \right)}$$

(60)

When $O_{2,ads} = O_{2xcess}$, $\lambda_{cat} = 1$.

The Data Base Catalyst Map – The performance characteristics of the catalyst can be obtained either on an engine dynamometer or in a chemical reactor. These experiments provide overall conversion efficiency across an entire catalyst of prescribed geometry, PM formulation/loading and degree of aging. The steady state conversion efficiencies of CO, HC and NOx (defined as $\eta_{cat}^{CO}, \eta_{cat}^{HC}, \eta_{cat}^{NOx}$, respectively) are correlated vs. a variety of inlet gas parameters that include temperature, air fuel ratio or lambda, flow rate, and emission gas concentration level. Using the steady state data in conjunction with the model, the average surface temperature, $\overline{T}_{w,map}$, is calculated for each mapping data point and included in the map. In general,

$$\eta_{cat}^{i} =$$

$$\eta_{cat}^{i}(\lambda, \overline{T}_{w}, \dot{m}_{g}, C_{g}^{i}, geometry, PM, aging, ...)$$

(61)

where i equals CO, HC or NOx.

Ideally, one could experimentally determine these conversion efficiencies as function of all the above mentioned parameters over a wide range of all possible conditions. However, to contain the total number of experiments and the corresponding facilities time to a practical value, the global conversion efficiencies of HC, CO and NOx are currently mapped for a single catalyst geometry and formulation as function of A/F ratio or lambda, for three inlet gas temperatures at three values of space velocity, and feedgas level concentration corresponding to a 4.6L 2V Ford engine.

Since the values of conversion efficiency are mapped over a finite range of conditions for a specific catalyst formulation, these efficiencies are interpolated when in the range of the experiments and extrapolated when outside the range at which they were obtained. The "core" part of a typical map is generated using inlet gas temperatures held constant at $T_{map(min)}$ = 380°C (720°F), $T_{map(mid)}$ = 450°C (840°F) and $T_{map(max)}$ = 510°C (950°F), while continuously varying A/F ratio from 1.0 A/F ratio lean of stoichiometry to 1.0 A/F ratio rich of stoichiometry at a space velocities of 85,000 hr⁻¹, 170,000 hr⁻¹, and 225,000 hr⁻¹. In addition to the core efficiencies obtained at constant inlet gas temperature, a "light-off" efficiency curve is generated which provides CO, HC and NOx efficiencies for a stoichiometric inlet gas which has its temperature slowly increased from ambient temperature to 380°C (720°F). A complete map for a particular PM formulation also includes data obtained for several PM loadings over the application range of these catalysts.

In all mapping completed to date, the performance data were obtained after the catalyst sample was aged on the current Ford aging cycle for 125 hours of exposure. This level of exposure is equivalent to a certain level of vehicle driven miles which varies depending on the particular catalyst formulation. Use of the model to predict the performance of a catalyst at a different age requires generation of another map. Nonetheless, a catalyst map for a single formulation and age can be used with appropriate scaling factors, discussed earlier, to account for differences between the mapped catalyst and the modeled catalyst in terms of space velocity, and catalyst geometry (such as monolith cell density and wall thickness).

Since our experiments yield global conversion efficiency for CO, HC and NOx and are obtained either at constant inlet gas temperature or at constant stoichiometry, we rewrite the global catalyst efficiency function in the following form which will lend itself to interpolation or extrapolation with a number of key variables.

$$\eta_{cat}^{i} = f_{scale}(\eta_{map}^{i}, SV, C_{g}^{i}, ..., etc.)$$

(62)

where f_{scale} is a scaling function (represented by Eq. 67 in the next section) that is used to adjust the efficiency interpolated from the map (η_{map}^{i}) for conditions different from those of the map. The map interpolation is performed in the following manner:

$$\eta_{map}^{i} = \frac{f_{map}^{i}(\lambda, \overline{T}_{w}')}{f_{map}^{i}(1, \overline{T}_{w}')} \cdot f_{Tmp}^{i}(\lambda = 1, \overline{T}_{w})$$

(63)

where:

f_{map}^{i} = core map efficiency

f_{Tmp}^{i} = light − off curve efficiency

$$\overline{T}_{w}' = T_{w,map(min)} \quad if \quad T_{w,map(min)} > \overline{T}_{w}$$

$$\overline{T}_{w}' = \overline{T}_{w} \quad if \quad T_{w,map(min)} < \overline{T}_{w} < T_{w,map(max)}$$

$$\overline{T}_{w}' = T_{w,map(max)} \quad if \quad \overline{T}_{w} > T_{w,map(max)}$$

(64)

which means that we interpolate directly within the core experimental data base if $T_{w,map(min)} < \overline{T}_{w} < T_{w,map(max)}$, and for surface temperatures outside the core experimental data base, an extrapolation is performed based on the shape of the ratio $f_{map}^{i}(\lambda, T_{w,map(min)}) / f_{map}^{i}(1, T_{w,map(min)})$ for surface temperatures lower than $T_{w,map(min)}$ or

$f_{map}^i(\lambda, T_{w.map(max)}) / f_{map}^i(1, T_{w.map(max)})$ for surface temperatures greater than $T_{map(max)}$. This preserves the shape of conversion efficiency as a function of A/F ratio (or λ) at all temperatures. $f_{Tmp}^i(\lambda = 1, \overline{T}_w)$ is obtained from the catalyst lightoff efficiency data obtained at stoichiometry. Efficiency data are then scaled for other parameters such as space velocity, and inlet gas concentration. Finally, while the ideal catalyst map would include performance data for a variety of PM loadings and catalyst ages, these data are not always readily available. Consequently, to provide a first order estimate of the potential impacts of PM loading or age differences, the scaling function developed for SIMTWC also contains terms which can be used to provide some insight into how these differences can also affect catalyst performance.

<u>Scaling Function</u> – The role of the scaling function is to extend the catalyst performance map to conditions occurring outside the performance map boundaries. This may include differences such as catalyst geometry, PM loading, age, inlet gas concentrations, and at the very least, flow rate (or space velocity). Since the catalyst map is obtained at a finite range of space velocities, a primary requirement of the scaling function is to predict performance at space velocities lower than 85,000 hr^{-1} and greater than 225,000 hr^{-1}. The following scaling for space velocity is applied and is based on the expressions specified previously (see Eq. 42).

$$\eta_{cat}^i = 1 - \left(1 - \eta_{map}^i\right)^{1/SV_{norm}} \tag{65}$$

where η_{map}^i is the mapped catalyst conversion efficiency at the mapped space velocity SV_{ref}, and η_{cat}^i is the estimated catalyst conversion efficiency for a normalized space velocity (SV_{norm}):

$$SV_{norm} = 3600 \cdot \dot{V}_g^{@STP} / (A_{face} \cdot L_{cat} \cdot SV_{ref}) \tag{66}$$

We extend Eq. 65 to the following generalized form of the scaling function to cover a wide variety of possible differences between the mapped catalyst and the catalyst being modeled.

$$\eta_{cat}^i = 1 - \left(1 - \eta_{map}^i\right)^{1/SF^i} \tag{67}$$

and SF^i is the overall scaling factor for species i that has the following form:

$$SF^i = SV_{norm}$$
$$\cdot \left(Age_{Ave}^i \cdot PM_{fac}^i \cdot GSA_{comp}\right)^{-1}$$
$$\cdot \left(PPM_{adj}^i \cdot SVCR^i\right)^{-1} \tag{68}$$

where:

Age_{Ave}^i is the average reduction in catalyst performance due to aging (for each species i) for the entire catalyst based on a user supplied performance reduction profile for individual catalyst elements.

PM_{fac}^i is an empirically based curve of the effect of PM loading and has the following format:

$$PM_{fac}^i = C1_{PM}^i + C2_{PM}^i * \exp\left(-C3_{PM}^i \big/ PM_{load}\right) \tag{69}$$

GSA_{comp} accounts for differences in geometric surface area:

$$GSA_{comp} = \frac{Ga}{Ga_{map}} \tag{70}$$

PPM_{adj}^i handles differences in inlet gas concentration that can affect catalyst performance, particularly in the case of species that follow a reaction mechanism more complex than first order.

$$PPM_{adj}^i = (C_g^i / C_{g(map)}^i)^{C_{ppm}^i} \tag{71}$$

and a final term, $SVCR^i$ is available to account for the varying effect space velocity has at different temperatures for each species i (included for future use, not currently exercised)

<u>Available Oxidant Limitations</u> – After the mapped efficiency is adjusted based on the scaling function, a final check is made to ensure that the reductant efficiencies have not exceeded the limit imposed by the amount of oxidant available. On the lean side, where there is an excess of oxygen, the reductant conversion efficiency is not affected by oxidant availability constraints. On the rich side, the deficiency of oxidants will place an overall limit on the possible conversion efficiencies of the reductants.

Due to small errors in the mapping process, it is assumed in the model that a lack of oxidants to fully react with the reductants will primarily impact the CO conversion (HC is given priority to react with the available oxidant). The following expressions are used to determine the maximum possible CO conversion imposed by oxidant limitations:

9

$$\eta^{CO}_{max} = \frac{\gamma - C^{HC}_g \cdot (2 + y/2) \cdot \eta^{HC}_{cat}}{C^{CO}_g + C^{H_2}_g}$$

(72)

$$\gamma =$$
$$\left[(C^{CO}_g + C^{H_2}_g) \cdot \eta^{CO}_{cat} + C^{HC}_g \cdot (2 + y/2) \cdot \eta^{HC}_{cat} \right] \cdot \alpha$$

(73)

$$\alpha = 1 / \text{Redox}_{ratio} / \eta_{red}$$

(74)

$$\text{Redox}_{ratio} = \frac{red_{in}}{ox_{in}}$$

(75)

$$red_{in} = C^{CO}_g + C^{H_2}_g + (2 + y/2) \cdot C^{HC}_g$$

(76)

$$ox_{in} = 2 \cdot C^{O_2}_g + C^{NO_x}_g$$

(77)

$$\eta_{red} = red_{burned} / red_{in}$$

(78)

$$red_{burned} = \eta^{CO}_{cat} \cdot (C^{CO}_g + C^{H_2}_g)$$
$$+ \eta^{HC}_{cat} \cdot (2 + y/2) \cdot C^{HC}_g$$

(79)

THE NUMERICAL SOLUTION

GENERAL CONSIDERATIONS – To analyze an emissions system using SIMTWC, component geometry and inlet gas temperature, A/F ratio, flow rate and species concentrations must be accurately specified. These feedgas values can be determined from other models which generate engine-out properties, or they can be obtained from vehicle experiments conducted over the appropriate drive cycle for analysis. Since all six inlet variables are necessary for calculation, the absence of an exhaust gas variable such as temperature will prevent accurate calculation. An average surface temperature and an average gas temperature are calculated in the catalyst element based on temperature distributions from the previous time step. Upon determining these average temperatures, an inlet value of A/F or λ_{inlet} is used in correspondence with the O_2 storage submodel to determine a new value for λ within the catalyst after O_2 is either added or removed from surface storage sites. After the new local value of λ is calculated, the catalyst performance map is interrogated at the appropriate A/F ratio, surface temperature and space velocity and a global catalyst efficiency is determined. From the global efficiencies, the local catalyst efficiency is determined based on the number of computational cells along the substrate and the species distribution is determined along the substrate. From this distribution of species, the local value of

$\dot{Q}_{chem.j}$ is determined and the gas and wall energy balances are calculated.

Since the output from one pipe/catalyst combination can be used as input to a downstream pipe/catalyst combination, a series of elements can be analyzed for any combination of exhaust system components. This is typically the approach used during a complete analysis of an exhaust system configuration.

EQUATION DISCRITIZATION – To solve the Eqs. 44-48, the length along the exhaust system is divided into number of longitudinal computational elements and these equations are approximated by their corresponding finite difference relations. The representations of the partial derivatives are obtained from Taylor series expansions in space and time and these expressions are shown below.

$$\frac{\partial T_w}{\partial t} = \frac{T^{n+1}_{w_j} - T^n_{w_j}}{\Delta t}$$

(80)

$$\frac{\partial T_g}{\partial z} = \frac{T^{n+1}_{g_j} - T^{n+1}_{g_{j-1}}}{\Delta z}$$

(81)

$$\frac{\partial C^i_g}{C^i_g} = \frac{C^{i,n+1}_{g_j} - C^{i,n+1}_{g_{j-1}}}{C^{i,n+1}_{g_j}}$$

(82)

For the conduction term in the solid, the second derivative of T_w with respect to z is written as:

$$\frac{\partial^2 T_w}{\partial z^2} = \beta_t \frac{(T^{n+1}_{w_{j-1}} - 2T^{n+1}_{w_j} + T^{n+1}_{w_{j+1}})}{(\Delta z)^2}$$
$$+ (1 - \beta_t) \frac{(T^n_{w_{j-1}} - 2T^n_{w_j} + T^n_{w_{j+1}})}{(\Delta z)^2}$$

(83)

where β_t is a weighting factor used to optimize calculation stability and accuracy. Normally, a value for β_t of 0.5 is used during calculation [see Hauffmann, K.A. (1989)]. Substitution of the Taylor series expansion and weighting factors into Eq. 44 yields:

$$-\dot{m}_g Cp_g \frac{(T^{n+1}_{g_j} - T^{n+1}_{g_{j-1}})}{\Delta z} =$$
$$h_i P_{l_{cat}} \left[\beta_z (T^{n+1}_{g_j} - T^{n+1}_{w_j}) + (1 - \beta_z)(T^{n+1}_{g_{j-1}} - T^{n+1}_{w_{j-1}}) \right]$$

(84)

where the change in gas temperature is equal to the weighted average heat flux from the gas to the wall. It should be noted that a spatial weighting factor, β_z is also used to optimize the accuracy of the calculation. Similar substitutions into Eq. 45 yield:

$$\rho_w A_{w_{cat}} C_{p_w} \frac{T_{w_j}^{n+1} - T_{w_j}^n}{\Delta t} =$$

$$h_I P_{I_{cat}} \left[(1 - \beta_t)(T_{g_j}^n - T_{w_j}^n) + \beta_t (T_{g_j}^{n+1} - T_{w_j}^{n+1}) \right] -$$

$$h_O P_{O_{cat}} \left[(1 - \beta_t)(T_{w_j}^n - T_{amb}) + \beta_t (T_{w_j}^{n+1} - T_{amb}) \right]$$

$$+ \frac{\lambda_w A_{w_{cat}}}{\Delta z^2} \left[\begin{array}{l} (1 - \beta_t)(T_{w_{j-1}}^n - 2T_{w_j}^n + T_{w_{j+1}}^n) \\ + \beta_t (T_{w_{j-1}}^{n+1} - 2T_{w_j}^{n+1} + T_{w_{j+1}}^{n+1}) \end{array} \right]$$

$$+ \dot{Q}_{chem} \tag{85}$$

The boundary and initial conditions are discretized as follows:

$$\frac{T_{w_2}^{n+1} - T_{w_1}^{n+1}}{\Delta z} = \frac{T_{w_{Ncell}}^{n+1} - T_{w_{Ncell-1}}^{n+1}}{\Delta z} = 0 \tag{86}$$

where N_{cell} is the last computational element along the substrate

$$T_{g_1}^n = T_{g,inlet}(t)$$

$$T_{g_1}^{n+1} = T_{g,inlet}(t + \Delta t) \tag{87}$$

$$T_{w_{j_.}}^0 = T_w^0(z) \tag{88}$$

$$C_g^i(0,t) = C_{g,inlet}^i(t) \tag{89}$$

The above equations are applied at each computation node along the pipe or along the catalyst elements and the following system of equations is constructed to obtain a solution for T_g and for T_w. This system of equations is solved simultaneously to obtain T_g and T_w. The solution of this system is obtained using a Gaussian diagonalization and back substitution algorithm.

$$A_j T_{g_{j-1}}^{n+1} + B_j T_{w_{j-1}}^{n+1} + C_j T_{g_j}^{n+1}$$

$$+ D_j T_{w_j}^{n+1} + E_j T_{g_{j+1}}^{n+1} + F_j T_{w_{j+1}}^{n+1} = G_j \tag{90}$$

SOLUTION PROCESS FOR A SINGLE TIME STEP

1. To start a calculation step, the gas, surface temperature, and $\dot{Q}$ arrays are initialized using the values from the previous time step or as specified at the start of the simulation.

2. The feedgas properties for a given time step of the simulation (temperature (K), A/F ratio, flowrate (kg/s), CO (kg/s), HC (kg/s), and NOx (kg/s) mass flow) are input, and the gas temperature for the first computation node is set according to Eq. 87.

3. An average surface temperature ($\bar{T}_w$) (based on the temperature distribution from the previous time step) is calculated considering only elements above a specified light-off temperature using Eq. 49. If none of the elements is above the specified light-off temperature, $\bar{T}_w$ is set equal to the maximum surface temperature within the catalyst.

4. From the inlet value of A/F (or λ), the exhaust gas oxygen excess or deficiency is calculated using Eq. 51.

5. Based on the result of Steps 3 and 4 and the degree of oxygen storage present on the catalyst, the fraction of oxygen adsorbed or desorbed by the catalyst is calculated using Eq. 59. This value is combined with the result from Step 4 to determine a new local value of λ_{cat} within the catalyst using Eq. 60.

6. A normalized space velocity (SV_{norm}) is calculated according to Eq. 66 based on the exhaust flow rate, catalyst volume, and the space velocity (SV_{ref}) used during the generation of the catalyst performance map.

7. The catalyst performance map is interrogated using the value of λ_{cat} calculated in Step 5, and the average surface temperature from Step 3 to determine global catalyst map efficiencies (η_{map}^i) for CO, HC, and NOx at SV_{ref} using Eq. 63.

8. The map efficiency, η_{map}^i is checked and clipped (if necessary) to ensure that it is within a lower limit of zero and an upper limit of one.

9. An overall scaling factor (SF^i) is calculated for each species i using Eq. 68 that incorporates several individual effects into a single parameter for each species. These individual effects include:

    a. Normalized space velocity from Step 6 (SV_{norm}).

    b. Catalyst age (Age_{Ave}^i): average reduction in catalyst performance (for each species i) for the entire catalyst based on a user supplied performance reduction profile for individual catalyst elements.

    c. Precious metal loading effects on each species i (PM_{fac}^i): calculated using Eq. 69

    d. GSA differences from the mapped catalyst (GSA_{comp}): calculated using Eq. 70

    e. Feedgas concentration levels for each species i (PPM_{adj}^i): calculated using Eq. 71

    f. The varying effect space velocity has at different temperatures for each species i ($SVCR^i$) (included for future use, not currently exercised)

11

10. The scaling function (Eq. 67) is used with the map efficiencies from Step 8 and the overall scaling factor from Step 9 to determine the overall global catalyst efficiencies possible without taking into consideration limitations imposed by the amount of oxidant available.

11. The efficiencies determined in Step 10 are compared to the maximum efficiencies possible based on available oxidant determined from Equation 72, and clipped if necessary to these maximum levels to provide the overall global efficiency (η^i_{cat}) for each species i.

12. Cell-by-cell local cumulative efficiencies for each species i ($\eta^i_{j,cum}$) up through cell j are calculated from the global efficiencies determined in Step 11 using Eq. 91.

$$\eta^i_{j,cum} = \left[1 - \left(1 - \eta^i_{cat}\right)^{1/SV^j_{effective}}\right]$$

(91)

where $SV^i_{effective}$ is determined from Eq. 92

$$SV^i_{effective} =$$

$$SF^i / (\sum_1^{j_{cum}} Age^i_j / Age^i_{Ave}) / j_{cum}$$

(92)

and Age^i_j = reduction in cell j conversion performance for species i due to aging.

13. The cell-by-cell local cumulative efficiencies for the reducing species, k, are used to calculate the exothermic heat, $\dot{Q}_{chem,j}$, generated within each computational element j using Eq. 93.

$$\dot{Q}_{chem,j} = \sum_k^{N_{red}} \left(\eta^k_{j_{cum}} - \eta^k_{j_{cum-1}}\right) C^k_g \dot{m}_{exh} \left(\Delta H_k\right)$$

$$for\, \eta^k_{j,cum} \le \eta^k_{cat}$$

$$\dot{Q}_{chem,j} = 0,$$

$$for\, \eta^k_{cat} < \eta^k_{j,cum}$$

(93)

where: ΔH_k is the heat of reaction k.

14. Knowing the energy released within each computational element as determined from Eq. 93, the system of equations represented by Equation 90 is solved simultaneously to obtain the gas and surface temperature distribution along the catalyst elements. An iterative calculation is used to handle the effects of the temperature dependent gas and wall properties (without updating the efficiency calculation or exothermic heat release) until a user specified convergence criteria is reached.

INPUT DATA PHYSICS (FEEDGAS SPECIFICATION)

A key input to SIMTWC is a precise characterization of the engine-out exhaust gas or "feedgas." More specifically, SIMTWC requires feedgas mass flow rate, temperature, HC, CO, and NOx level, and A/F ratio (or oxygen content) as a function of time during a drive cycle of interest. Ideally, this information can be provided by either another simulation model, or actual test measurements. However, many engine feedgas simulation programs are valid only for fully warmed-up engine operation, and in many cases, it is the transient cold-start and warm-up portion of the emission cycle that dominates overall emission performance. Therefore, in most cases, SIMTWC must rely on test measurements to provide the needed feedgas information over the drive cycle of interest.

Several emission test facilities routinely measure most of the information required by SIMTWC. While the measurement techniques used to characterize the feedgas are sufficient for many types of emission assessment/calibration work, there are several areas in which the measurements do not adequately reflect the true exhaust feedgas with the precision required by SIMTWC. Like a real catalyst, SIMTWC is extremely sensitive to minute changes in feedgas constituents, and in order to obtain meaningful results from SIMTWC, it is very important that the input to the model reflect the actual feedgas quality as closely as possible.

By understanding what causes the inaccuracies in the feedgas measurements, it is possible to make some adjustments to the reported feedgas values to more accurately reflect the true exhaust make-up. Five known causes of measurement inaccuracies are discussed below together with techniques to compensate for them.

TEMPERATURE MEASUREMENTS – Thermocouples are the typical temperature sensors used to measure exhaust gas temperature (T_g) in dynamometer and vehicle experiments. They are comprised of the junction of two wires of dissimilar materials which contains thermal mass. The temperature reported by the thermocouple is actually that of the of the thermocouple junction (T_{TC}) and not necessarily that of the surrounding environment due primarily to the thermal inertia of the junction mass. The response lag of the thermocouple to changes in the exhaust gas temperature is a function of the thermocouple size and exhaust flow rate. By using a simple model of thermocouple energy conservation as suggested in Figure 2, it is possible to account for the effects of thermocouple mass and to obtain a better estimate of the actual exhaust gas temperature. This is done by taking into account the heat transfer between the exhaust flow and the thermocouple junction and writing the corresponding energy balance between the thermocouple junction and the gas flow. This yields:

$$m_{TC} Cp_{TC} \frac{dT_{TC}}{dt} = -h_j A_{TC} \left(T_{TC} - T_g \right)$$

$$\frac{dT_{TC}}{dt} = -\frac{h_j A_{TC}}{m_{TC} Cp_{TC}} \left(T_{TC} - T_g \right)$$

(94a)

$$\frac{1}{\tau} = \frac{h_j A_{TC}}{m_{TC} Cp_{TC}}$$

$$T_g = T_{TC} + \tau \frac{dT_{TC}}{dt}$$

(94b)

where τ, in general, is a function of the exhaust flow rate and thermocouple size.
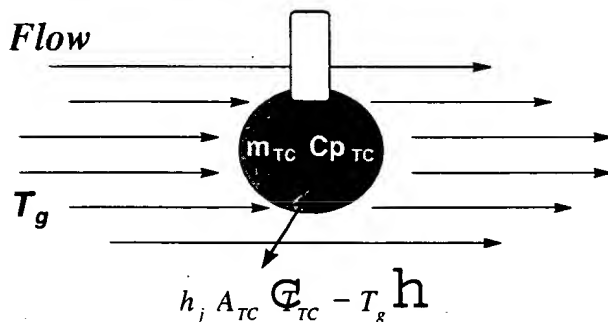
Thermocouple Energy Balance

Figure 2. Schematic of thermocouple energy exchange process.

Experience has shown that for the range of exhaust flow rates encountered during a standard EPA Federal Test Procedure (FTP), τ is nearly independent of flow rate, and use of a constant value for a given thermocouple size is sufficient for calculation. Values for τ range from 4 seconds for a 1/16" thermocouple to 8 seconds for a 1/8" thermocouple. For simulations of cycles that involve higher exhaust flow rates (such as the US06 in the Supplemental FTP), it is necessary to take into account the effect of flow rate on τ.

EXHAUST FLOW MEASUREMENTS – Exhaust flow measurements at many emission test facilities are made using the CO_2 tracer method. This method relies on a measurement of engine out CO_2 concentration obtained from an analyzer which is located remotely from the test vehicle (~10 m). Due to the inherent time delay associated with the transport of the exhaust sample to the emission analyzer, the CO_2 tracer technique generally underestimates the engine flow dramatically during the first 5 to 15 seconds of an emission test. This underestimate of flow is extremely important, since it also leads to an underestimate of the calculated energy transport from the engine to the emissions system, thus lengthening the calculated time of catalyst lightoff in the emissions system. It is therefore necessary to correct the exhaust flow

determined with the CO_2 tracer technique during the early part of a test using other exhaust measurement techniques, such as the Smooth Approach Orifice (or SAO) or other engine parameters such as rpm, load, and manifold vacuum – a speed-density calculation of flow.

Additionally, in many facilities, flow estimates from the CO_2 tracer technique are reported as the dry exhaust flow rate (total exhaust flow minus the water content). Because typical gasoline exhaust contains about 12-13% water, use of the dry exhaust flow rate would result in a significant underestimation of the amount of sensible heat delivered to the catalyst during the light-off portion of the emission test. Consequently, the dry exhaust flow is increased to account for the water content before the data is fed into SIMTWC.

STOICHIOMETRIC AIR/FUEL RATIO DETERMINATION – Transient Air/Fuel ratio (A/F) is generally calculated from data obtained using conventional emissions analyzers or measured with a UEGO (universal exhaust gas oxygen) sensor during an emission test. It is not unusual for measurements using these devices to be shifted slightly rich or lean (± .05) of the exhaust's actual A/F as a result of inaccuracies in instrument calibration, fuel hydrogen/carbon fluctuations, sampling delays, and only partial mixing of the exhaust gas from all engine cylinders. Inaccuracies of this order may appear small compared to typical exhaust A/F of 14.6:1 for gasoline. However, when attempting to determine the relative oxygen content of the exhaust which involves the difference between the measured A/F and the stoichiometric A/F, measurement shifts of this order can have a tremendous impact on the accuracy of calculation. Consequently, it is necessary to carefully analyze each data set to determine whether there is an offset between the measured A/F ratio and the actual A/F ratio.

In our process, an initial estimate of the offset in A/F ratio is obtained by averaging the measured A/F ratio values during a section of the test when the engine is known to be fully warmed-up and remains in closed-loop operation. At this condition, the A/F ratio should be near to the stoichiometric A/F ratio as determined from the H/C and O/C ratios of the fuel. If there is a difference between the measured average A/F ratio and the stoichiometric A/F ratio calculated from fuel properties, the difference is eliminated for the entire emissions test. In addition, if a baseline emission test with tailpipe measurements is available, it is possible to make refinements to this initial estimate by comparing the ratio of tailpipe CO/NOx mass predicted by SIMTWC to that actually measured.

TIME ALIGNMENT OF SIGNAL TRACES – During an emission test, the exhaust sample passes through several different sensors/analyzers to determine the mass flow, temperature, and A/F, HC, CO, and NOx levels. Generally, an attempt is made at the emission facility to time align the signals from the various detectors; how-

ever, in most cases, a more refined alignment is required to get the most meaningful results from emissions models. Currently, we take advantage of the strong correlation between exhaust mass flow, temperature, and feedgas NOx mass flow rate that generally exist to align these three signals. We then assume that the HC and CO signals are aligned with the NOx, and finally use the strong correlation between CO concentration and A/F to align the A/F with all signals.

"FILTERED" EMISSION SIGNALS – In many emission facilities, the CO, HC, and NOx concentrations are measured by analyzers which are located at least 10m away from the test vehicle. Because of the long sample lines, a degree of mixing or filtering of emissions constituents occurs by the time the exhaust sample reaches the emission analyzers. In experiments using a closely-located HC analyzer, known as the "Fast-FID" [Summers T. and Collings, N (1995)], this instrument has shown repeatedly the dramatic difference between the actual exhaust HC concentration and that measured by the standard remote analyzer. Again, to get the best possible results from SIMTWC or other emissions models, it is imperative to know the emission concentrations entering the catalyst as precisely as possible.

Use of the Fast-FID is helpful, but it is not standard practice at most facilities. In addition, other "Fast" instruments are needed. Fast-NOx analyzers are another example of instrumentation which shows dramatic differences with conventional analyzers and are being evaluated. In the interim, we are investigating methods to "unfilter" the emission signals using techniques similar to that used for the thermocouple signal. However, at this time, a standard technique has not yet been adopted.

RESULTS AND DISCUSSION

MODEL COMPARISON WITH VEHICLE EXPERIMENTS – To assess modeling accuracy, SIMTWC was used to calculate catalyst performance and the corresponding accumulated emissions over several vehicle test cycles for a variety of different test vehicles and catalyst configurations as listed in Table I. In addition to those listed in Table I, other variable changes included catalyst position, catalyst cell density, catalyst PM loading, exhaust system geometry, catalyst aging, and fuel type (California reformulated and Indolene). All calculations were done with fixed calibration of the model to determine the amount of difference between experiment and model calculation over a wide range of conditions and emissions levels.

Table I. Vehicle and Drive Cycle Combinations

Vehicle	Engine	Drive Cycle
Grand Marquis	4.6L V8	FTP
Town Car	4.6 L V8	FTP, MVEuro, & US06
Contour	2.0L I4	FTP
Heavy-Duty F-Series Truck	6.8L V10	Heavy-Duty Gas Engine Test
Lincoln LS	4.0L V8	FTP

Figure 3 shows the values predicted by SIMTWC when compared to those measured during experiment. The values on the abscissa represent the accumulation of transient experimental "modal" data obtained on a second-by-second basis throughout a typical vehicle-on chassis dynamometer experiment. The ordinate represents the accumulated tail pipe emissions as calculated by SIMTWC (open square markers). The solid straight line would represent perfect agreement between experimental results and theoretical predictions. The two outer dotted lines indicate a difference of 30% between the modal measurements and the SIMTWC prediction. Herein, most predictions by SIMTWC lie within 30% of the measured values for all combinations of test conditions and geometries that generate emission levels that span several orders of magnitude in value.

To help put this into perspective, Figure 3 also shows the corresponding "bag" emission values measured during these experiments (solid triangle markers). Note that the values from the bag measurements vary from the values of the measured modal results by approximately the same degree as the model prediction, thus suggesting that the error generated from the model is similar to the error which is generated during experiment. Moreover, remember that these bag measurements were obtained during the same experiment as the accumulated modal measurements, using the same experimental facility and vehicle emissions system, and still the difference in measurements is similar to the difference between model and experiment. Also, remember that the catalyst representation in the model reflects the performance of an average aged catalyst and does not exactly represent the catalyst on any one particular vehicle due to manufacturing variability, differences in catalyst aging (ADP/fleet), degree of contamination, and so on. Performance differences due to differences in aging are also discussed later.
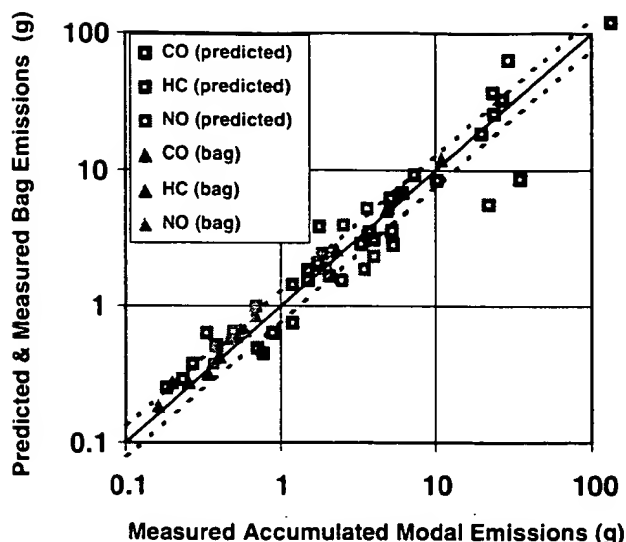
Figure 3. Comparison of predicted and measured emissions

Figure 4. Exhaust system geometry

Figure 5. Accumulated emissions over the FTP drive cycle at midbed and tailpipe positions for TownCar Config. A.

Figure 4 shows two vehicle geometries, which are derivatives of the Lincoln TownCar production geometry, used during calculations to compare second-by-second CO, HC and NOx emissions at catalyst midbed and tailpipe positions.

Using configuration A and the appropriate feedgas input, the results in Figure 5 show the accumulated CO, HC, and NOx emission level during bags 1 and 2 of FTP cycle as a function of time at both midbed and tailpipe locations. These accumulated sec-by-sec emissions show good correlation between the predicted and measured values at the midbed catalyst location. Here, they are within 30% of one another, with the difference in measured and calculated HC within 10%. However, at the tailpipe position, the measured NOx emission is 50% lower than the calculated NOx emission. This is in part due to the fact that the lead catalyst was aged in the same manner as the catalyst used to generate the performance map in the model, whereas the second and third catalysts on the vehicle were aged behind the first catalyst as a system and experienced significantly different aging conditions than the first catalyst (e.g., lower inlet gas temperatures, little exotherm on the catalyst and reduced chemical poisons). This combination of factors suggests less deterioration of the rear catalyst bricks and is consistent with the higher NOx emissions produced during calculation. Since the current model calibration yields higher NOx emissions for rear catalyst position (a lower NOx efficiency), it acts as a conservative estimate of the tailpipe emission for the system. In addition, this suggests that an additional calibration should be undertaken for catalyst in the rear brick position and should be dependent on the temperature history of these catalyst which, in turn, is dependent on their location in the emissions system.
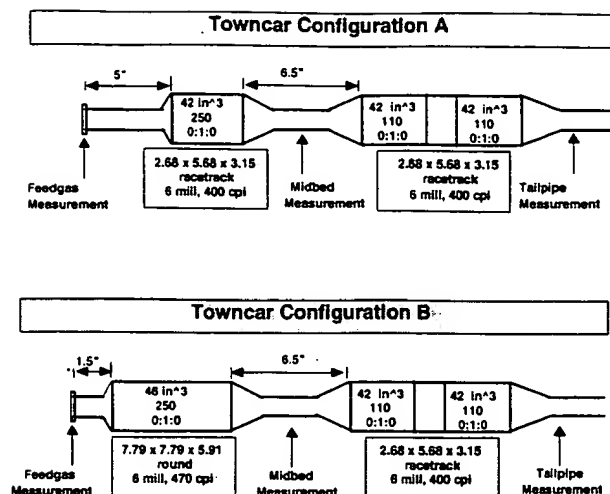
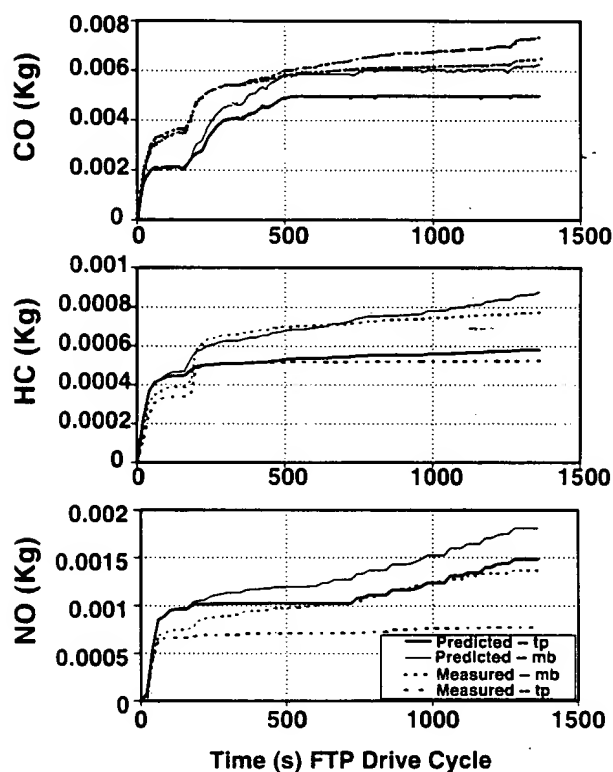In Figure 6, the instantaneous CO, HC and NOx conversion efficiencies (([]$_{in}$ - []$_{out}$)/ []$_{in}$ x 100) are plotted versus time at the midbed catalyst position for the first 200 seconds of the FTP drive cycle for TownCar configuration A. In general, they follow similar trends with experiment. However, for the first 10 to 20 seconds of the cycle, the measured efficiencies rose to unreasonably high values considering the catalysts were cold when the experiment started, and they (the efficiencies) dropped to negative values (not plotted) within a short period of time after

15

vehicle start. This behavior suggests the absorption and release of unreacted emissions species by the catalyst during its initial warm up. Since these experiments show little occurrence of reaction, the absorption/desorption simply acts as a time delay of emissions species without change in their total value and this effect is currently not considered in the SIMTWC model. A future SIMTWC element will be developed to account for this phenomenon. Many of the differences incurred between measured and calculated efficiency after this initial warm up period are due to the lack of precise alignment of AF ratio with emission measurements and are also due to the effect of filtered measurements of emission signals. Moreover, when the feedgas concentration of a given emissions species is small, the error in calculating efficiency is greater. This is partly due to the accurate measurement of a small emissions concentration and its placement in the denominator during the efficiency calculation. As noted in the previous plot this has little effect on the accumulated mass emission from the vehicle, since the feedgas emission levels are extremely low during these periods.
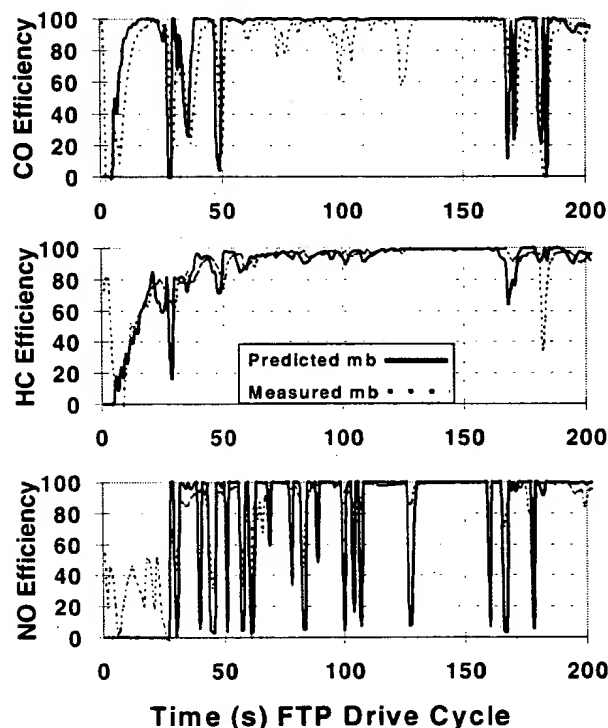

Figure 6.   Instantaneous CO, HC and NOx efficiency at midbed and tailpipe positions for TownCar Config A.

As in Figure 5, Figures 7 and 8 show a comparison between calculated and measured accumulated CO, HC and NOx midbed and tailpipe emissions when drive cycle is changed (Figure7; TownCar configuration A; US06 drive cycle) and when emissions system geometry (Figure 8; TownCar configuration B: FTP drive cycle) is changed. As seen, the absolute emissions levels have changed in correspondence with driving cycle and with geometry.

In Figure 7, the calculated NOx emission is in good agreement with measurement on the US06 drive cycle which does not contain a vehicle cold start. The calculated HC emissions is within 30% ({1 - .68/.95}x100) of measurement. Since the regulation for the US06 drive cycle is a composite of the HC and NOx emissions and since the NOx emissions, as seen in Figure 7, is generally an order of magnitude greater than the HC emission, the calculated US06 HC+NOx composite emission is in excellent agreement with measurement.
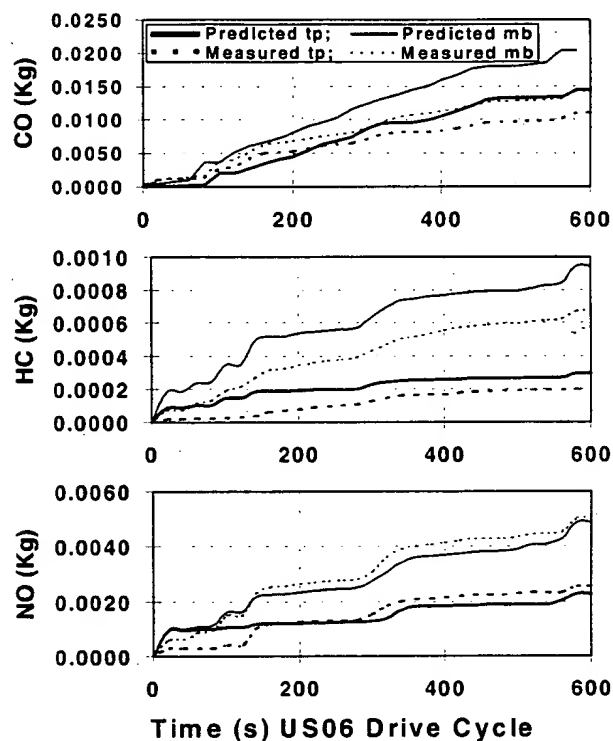

Figure 7.   Accumulated emissions over the US06 drive cycle at midbed and tailpipe positions for TownCar Config. A.

Figure 8 shows a comparison between the calculated and measured emissions generated by TownCar configuration B. Here, geometry has changed from the baseline configuration A. In this configuration, the catalyst is closer to the engine, the volume of the catalyst is greater (46 vs. 42 in^3), its cell density is higher (470 vs. 400 cpsi), the catalyst shape has changed (round vs. oval), the feedgas signatures are different, and it has been aged at a different time than the baseline configuration. Yet, SIMTWC has accounted for these changes. As in Figure 5, Figure 8 shows smaller differences across the lead catalyst and larger differences across the rear catalyst. Again, this catalyst experienced significantly different aging conditions than those used to age the lead catalyst and those used to age the catalyst to generate the performance map for the model. As seen in Figure 8, the largest difference is in the NOx tailpipe emission; it is within 35% ({1 -

16

.08/.12}x100) of measurement. Again, the current calibration in SIMTWC yields a conservative (slightly lower NOx efficiency) estimate of the tailpipe emission.
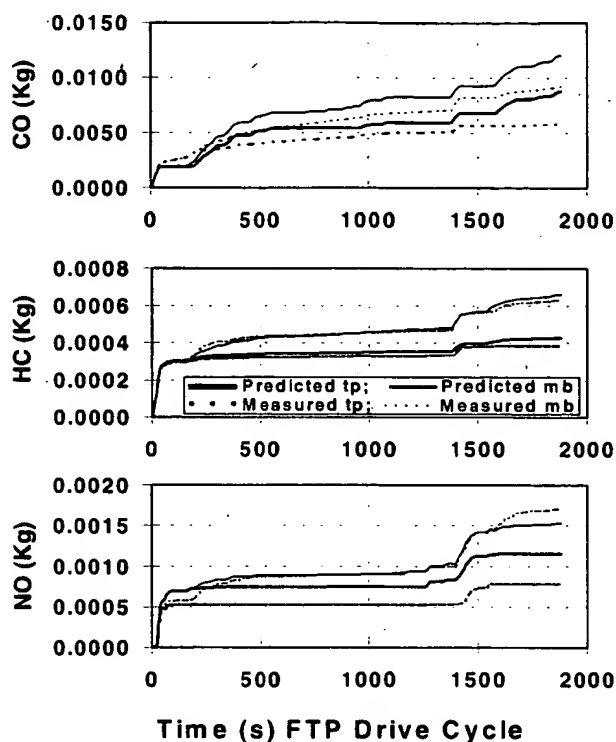

Time (s) FTP Drive Cycle

Figure 8. Accumulated emissions over the FTP drive cycle at midbed and tailpipe positions for TownCar Config. B.

MODEL SENSITIVITY – SIMTWC contains all the sensitivities of catalyst and emission system behavior. As an example, if one biases A/F ratio by an extremely small amount, the emissions system efficiency will change appropriately. If geometry, or materials of the catalyst change, the appropriate material properties are incorporated into the model. If engine spark timing or air/fuel ratio is varied as a method of engine control, the model reflects this engine control, since the feed gas time signature used as input to SIMTWC has incorporated the appropriate information to account for this control. In this section, we give a few examples of performance changes with catalyst location change and A/F ratio bias change.

Using TownCar configuration B as a baseline and its corresponding feed gas data set over bags 1&2 of the FTP drive cycle, the changes in tailpipe emissions levels and emission system temperature are shown in Figures 9-11 as catalyst location is changed and as A/F ratio is biased relative to stoichiometry.

Figure 9 shows the effect of changing the position of the lead catalyst from its base line location (1.5" downstream of the manifold flange, see Figure 4) to 0.3m ahead of the manifold flange and to 0.6m downstream of it. Note that, when the position of the first catalyst was moved downstream and reached the position of the second catalyst, the entire catalyst system was relocated downstream

appropriately. As seen in Figure 9, there is a 6x (0.06/0.01) increase in the tailpipe HC emission, a 2x (0.7/0.35) increase in the CO emission, and a 50% ({0.16/0.11 -1}x100) increase in the NOx emission when the lead catalyst location is changed over this range. The large increase in the HC and CO emissions is due to retarded catalyst lightoff which is due to less sensible heat arriving at the catalyst. The smaller increase in NOx is due to lower temperature at the catalyst during steady state operation.
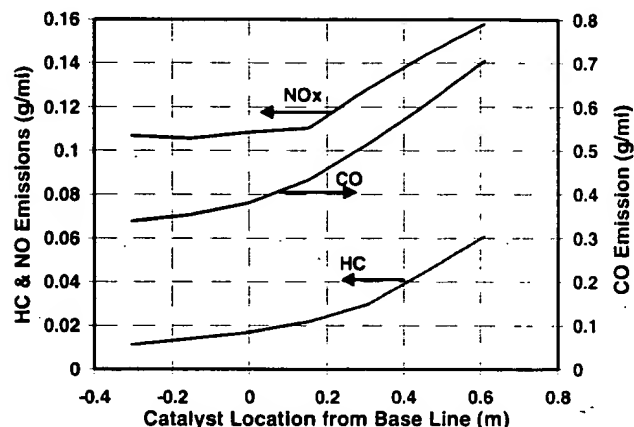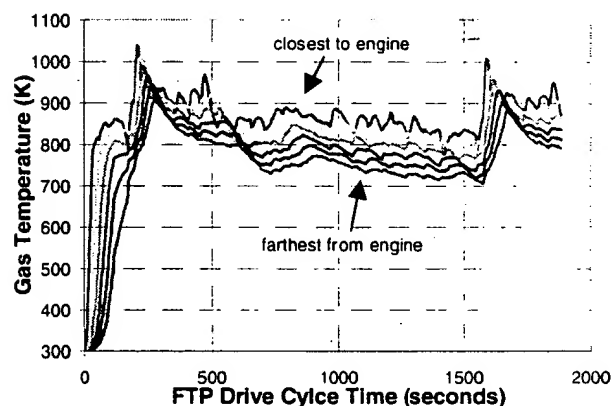

Figure 9. Emissions with change in catalysts

Figure 10. Feedgas temperature into 1st catalyst used in Figure 9. Higher temperatures correspond to the shortest distance from the engine. Distances correspond to those used in Figure 9

Figure 10 shows how the feedgas temperature to the lead catalyst changes when the location of catalyst is changed as above. As seen, when the lead catalyst is at its closest position, the inlet gas temperature is approximately 15% higher than when it is at its most downstream location. This is extremely important, since it affects catalyst lightoff, hence emissions, and also affects catalyst deterioration due to high temperature exposure. Therefore, a tradeoff between lightoff performance and catalyst deterioration ultimately determines the optimum location for the lead catalyst, since the emissions system must perform well at 120K vehicle miles.

17

Since a small bias in A/F ratio strongly affects emissions performance, we show the effect of AF ratio bias on tailpipe emissions for this catalyst configuration. Here, we artificially shift A/F ratio either lean or rich of the baseline A/F ratio indicated as zero bias on Figure 11. As seen in Figure 11, the CO emission increases 3x (1.2/0.4) when A/F is biased rich by 0.02 A/F and the NOx increases by 80% ({0.18/0.1-0.1}x100) when the A/F ratio is biased lean by a corresponding amount. Remembering that these increases are specifically related to the exact A/F ratio-time signature studied, the amount of increase or decrease can change dramatically from these levels. An important point to remember is that the specification of A/F ratio by experiment or by other upstream models of engine performance or control strategy must be within ±0.1% (0.02/14.6) of the actual A/F ratio or the tailpipe emissions can be in error by 100%. This accuracy suggests the importance of A/F ratio specification or measurement as all calibration specialists know.
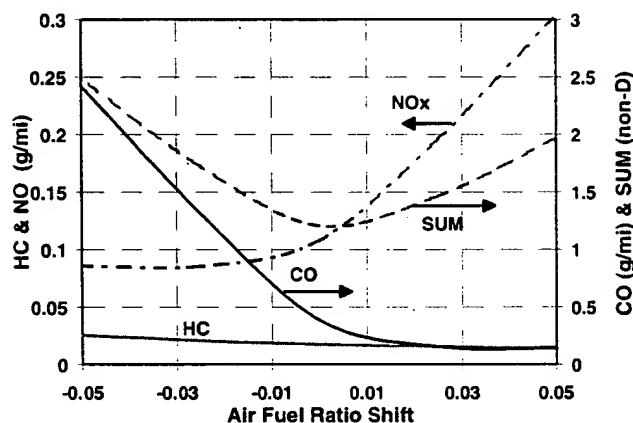

Figure 11. Effects of Air-to-Fuel ratio bias on tailpipe emissions over the FTP drive cycle for TownCar Configuration A. SUM indicates the sum of all three emissions constituents after normalization with the ULEV emissions targets (HC=0.04; CO=1.7; NOx=0.2).

In addition to the variation of each individual emissions species, the sum of all three species after normalization with the ULEV emissions targets (HC=0.04g/mi; CO=1.7g/mi; NOx=0.2g/mi) is shown. Thus

$$SUM = \frac{CO}{1.7} + \frac{HC}{0.04} + \frac{NOx}{0.2}$$

and is non-dimensional. The rescaling of emissions species is done to provide equal weighting before summation. This value shows a minimum very near the zero bias point, suggesting that the overall A/F ratio measurement is correct and the vehicle calibration is appropriate for minimum emissions over the FTP cycle.

CONCLUDING REMARKS

A simple tailpipe emission prediction model (SIMTWC) has been developed by combining fundamental conservation expressions for mass and energy with a first order oxygen storage model and an empirical data base of steady-state catalyst performance obtained during engine dynamometer assessments. SIMTWC offers several advantages over more complicated techniques including computational expedience and robustness with accuracy usually better than 30% for all emission species and over various drive cycles. Using this approach, an FTP emission cycle for a six pipe plus six brick emission system can be modeled on a 233 MHz Pentium™ II PC in less than three minutes. This provides an engineer the ability to rapidly evaluate many geometries and operating strategies. Updates to SIMTWC as catalyst formulations change are also accomplished in a relative easy and timely manner making SIMTWC is an extremely useful tool which offers the ability to sort through major aftertreatment design and strategy alternatives quickly while assisting in the interpretation of experimental data.

ACKNOWLEDGMENTS

REFERENCES

1. Gandhi, H.S., Delosh, R.G., Piken, A.G., and Shelef, M., "Laboratory evaluation of three-way catalysts," S.A.E. Transactions, Vol 85, Sec. 2, p. 201, The Society of Automotive Engineers, (1976).

2. Koltsakis, G.C., Konstantinidis, P.A., Stamatelos, A.M., "Development and application of mathematical models for 3-way catalytic converters," Applied Catalysis B: Environmental, Vol 12, p 161-191, (1997).

3. Hauffmann, K.A., Computational Fluid Dynamics for Engineers, Engineering Education System(TM), Austin, TX, 1989.

4. Li, P., Adamczyk, A.A. and Pakko, J.D., "Thermal Management of Automotive Emission Systems: Reducing the Environmental Impact", Thermal Engineering for Global Environmental Protection, ISBN 1-56700-055-X, Begell House, Inc, Publishers, New York, Wallington (UK), p 55-77 (1996), Ed. S. Sengupta.

5. Montreuil, C.N., Williams, S.C. and Adamczyk, A.A., "Modeling current generation catalytic converters: Laboratory experiments and kinetic parameter optimization -- Steady state kinetics," S.A.E. Paper No. 920096, The Society of Automotive Engineers, (1992).

6. Oh, S.H., Cavendish, J.C., and Hegedus, L.L., "Mathematical modeling of catalyst converter lightoff: single pellet studies," AiChE Journal, Vol 26, No. 6, p 935, (1980).

7. Otto, N.C. and LeGray, W.J., "Mathematical models for catalytic converter performance," S.A.E. paper No. 800841, The Society of Automotive Engineers, (1980).

8. Summers T., Collings, N., 'Modeling the Transit Time of a Fast Response Flame Ionization Detector During In-Cylinder Sampling," S.A.E. Paper No. 950160, The Society of Automotive Engineers, (1995).

NOMENCLATURE

a_I = internal heat transfer coefficient augmentation factor (dimensionless)

a_O = external heat transfer coefficient augmentation factor (dimensionless)

A_{face} = facial area of the catalyst substrate (m^2)

= $Hgt \cdot CC + \pi \cdot Hgt^2 / 4.0$

(racetrack geometry)

A_{TC} = thermocouple surface area (m^2)

$A_{w_{pipe}}$ = cross-sectional area of pipe wall (m^2)

$A_{w_{cat}}$ = solid cross-sectional area of catalyst (m^2)

Age_{Ave}^i = average reduction in catalyst performance due to aging for species i

$C1_{PM}^i$ = precious metal loading function constant for species i

$C2_{PM}^i$ = precious metal loading function constant for species i

$C3_{PM}^i$ = precious metal loading function constant for species i

C_0^i = initial catalyst concentration of species i at time t=0

C_{ppm}^i = constant for species i used in the inlet concentration adjustment factor

C_g^i = gas concentration of species I (g-mole/m^3 @ STP)

$C_{g,inlet}^i$ = inlet gas concentration of species I (g-mole/m^3 @ STP)

$C_{O_2 store}^i$ = O_2 storage concentration of species i (g-mole/m^3 @ STP)

$C_{O_2 store}^{Tot}$ = Total O_2 storage concentration (g-mole/m^3 @ STP)

$C_{w_j}^i$ = surface concentration of species i at location j (g-mole/m^3 @ STP)

$C_{w\ inlet}^i$ = surface concentration of species i at the inlet of the catalyst (g-mole/m^3 @ STP)

$C_{w,outlet}^i$ = surface concentration of species i at the outlet of the catalyst (g-mole/m^3 @ STP)

CC = $W - Hgt$ (m) (racetrack geometry)

CD = cell density (cells/m^2)

Cp_g = heat capacity of the exhaust gas
= (J/Kg/K)

$962.097 + 0.1507 \cdot T_g(K)$

Cp_{TC} = thermocouple heat capacity (J/Kg/K)

Cp_w = wall heat capacity (J/Kg/K)

= heat capacity of ceramic (J/Kg/K)

$Cp_{w(cer)}$ = $1071.0 + 0.156 \cdot T_w(K) - \dfrac{3.435 \cdot 10^7}{T_w(K)^2}$

$Cp_{w(Fe)}$ = heat capacity of iron (J/Kg/K)
= 460.52

$Cp_{w(SS)}$ = heat capacity of stainless steel (J/Kg/K)
= 502.39

$Cp_{w(Fe)}$ = heat capacity of steel (J/Kg/K)
= 502.39

= catalyst cell hydraulic diameter (m)

$D_{l_{cat}}$ = $\dfrac{1}{\sqrt{CD}}\left(1.0 - W_t\sqrt{CD}\right)$

$D_{l_{pipe}}$ = inside pipe diameter (m)

$D_{O_{pipe}}$ = outside pipe diameter (m)

f_{map}^i = core map efficiency of species i

f_{Tmp}^i = light-off curve efficiency of species i

f_{scale} = scaling function to extrapolate conversion efficiencies outside performance conditions

g = gravitational acceleration (m/s^2)
= 9.807

= geometric surface area (m^2/m^3)

Ga = $4.0 \cdot \left(1.0 - W_t\sqrt{CD}\right)\sqrt{CD}$

Ga_{map} = geometric surface area of mapped catalyst (m^2/m^3)

Gr = Grashof Number

GSA_{comp} = ratio of modeled catalyst geometric surface area to mapped catalyst surface area

Hgt = height of substrate face (m) (racetrack geometry)

h_I = internal heat transfer coefficient (J/m^2/s/K)

h_j = heat transfer coefficient between flow and thermocouple (J/m^2/s/K)

h_O = external heat transfer coefficient (J/m^2/s/K)

$k_{release}$ = release rate constant for oxygen storage

k_{store} = storage rate constant for oxygen storage

k_m^i = mass transfer coefficient of species i (m/s)

19

L_{cat} = length of catalyst (m)

$L_{cat(active)}$ = length of catalyst that has a temperature above a specified light-off value (m)

L_{pipe} = length of pipe (m)

$\dot{m}_{xcess}$ = normalized molar flow rate of excess/deficient oxygen into the catalyst

$\dot{m}_{exh}$ = exhaust gas molar flow rate (g-mole/s)

$\dot{m}_g$ = exhaust gas mass flow rate (Kg/s)

$\dot{m}_{g,inlet}$ = inlet exhaust gas mass flow rate (Kg/s)

m_{TC} = thermocouple mass (Kg)

Mw_g = exhaust gas molecular weight (Kg/g-mole)
= 0.028966

n_{order} = reaction rate order

N_{cell} = number of computational cells per exhaust system component

$N_{cell(active)}$ = number of computational cells having a temperature above a specified light-off value

N_{react} = number of reactions

N_{red} = number of reductant species

$N_{species}$ = number of species

Nu_I = Nusselt Number (inside)

$Nu_{I(laminar)}$ = Laminar Nusselt Number (inside)

$Nu_{I(turbulent)}$ = Turbulent Nusselt Number (inside)

Nu_O = Nusselt Number (outside)

ox_{in} = measure of total oxidant concentration within the catalyst (g-mole/m^3 @ STP)

$O_{2,cap}$ = oxygen storage capacity (g-moles O_2/Kg catalyst)

$O_{2,ads}$ = mole fraction of oxygen adsorbed or desorbed by the catalyst

O_{2xcess} = exhaust gas oxygen excess or deficiency (mole fraction)

P_g = Gas pressure (Pascal)

$P_{I_{cat}}$ = total catalyst cell inside perimeter (m)
= $4 \cdot D_{I_{cat}} \cdot CD \cdot A_{face}$

$P_{O_{cat}}$ = catalyst outside perimeter (m)
= π Hgt + 2 CC (racetrack geometry)

$P_{I_{pipe}}$ = pipe inside perimeter (m)
= $\pi D_{I_{pipe}}$

$P_{O_{pipe}}$ = pipe outside perimeter (m)
= $\pi D_{O_{pipe}}$

PM_{fac}^i = empirical function which describes the effect of PM loading on species i conversion

PM_{load} = PM loading (Kg/m^3)

PPM_{adj}^i = concentration effect factor for species i

Pr = Prandtl number of exhaust gas at T_g

$\dot{Q}_{chem}$ = rate of heat generated by chemical reaction per unit length of catalyst (J/m-s)

$\dot{Q}_{chem,j}$ = rate of heat generated in cell j by chemical reaction per unit length of catalyst (J/m-s)

red_{burned} = measure of total reductant concentration consumed (g-mole/m^3 @ STP)

red_{in} = measure of total reductant concentration within the catalyst (g-mole/m^3 @ STP)

r_{T_w} = reaction rate constant at T_w

R = gas constant
= 8.314 J/g-mole/K

Re = Reynolds number

R_k = rate of reaction of the kth reaction per unit surface area (g-mole/m^2/s)

R^i = overall rate of reaction for reactions involving species i (g-mole/m^2/s)

$Redox_{ratio}$ = redox ratio
= red_{in} / ox_{in}

S_{ext} = external surface-to-volume ratio (m^2/m^3)
= $P_{O_{cat}} / A_{face}$

SF^i = overall scaling factor for species i (dimensionless)

SV = space velocity (hr^{-1})
= $3600 \cdot \dot{V}_g^{@STP} / (A_{face} \cdot L_{cat})$

$SV_{effective}^i$ = effective space velocity taking into account aging and the overall scaling factor (hr^{-1})

SV_{norm} = normalized space velocity (dimensionless)
= SV / SV_{ref}

SV_{ref} = reference space velocity (hr^{-1}) used during the mapping of the catalyst.

$SVCR^i$ = space velocity vs. temperature adjustment factor for species i

T_f = film temperature (K)
= $(T_g + T_w)/2$

$T_{g_z}^t$ = exhaust gas temperature at position z and time t (K)

$T_{g,inlet}(t)$ = Inlet gas temperature at time t (K)

T_{map} = Inlet mapping gas temperature (K)

T_{TC} = thermocouple junction temperature (K)

$T_{w_z}^t$ = surface temperature at position z and time t (K)

20

$T_{w_z}^0$	=	Initial wall temperature at position z (K)
T_z^0	=	Initial temperature distribution at time=0
$\overline{T}_w$	=	average catalyst surface temperature of cells above a specified light-off temperature (K)
$\overline{T}_{w,map}$	=	calculated average catalyst surface temperature under mapping conditions (K)
T_{amb}	=	ambient temperature (K)
t	=	time (s)
v_g	=	local gas velocity along the catalyst (m/s)
$\dot{V}_g$	=	volumetric gas flow rate (m³/s)
W	=	width of substrate face (m) – (racetrack geometry)
W_t	=	cell wall thickness (m)
y	=	fuel hydrogen to carbon ratio
z	=	axial position along length of the pipe or catalyst (m)
$\overline{z}$	=	normalized position along length of the catalyst (dimensionless)
	=	z / L_{cat}

Greek Symbols

α	=	available oxidant calculation variable
	=	expansion coefficient (1/K)
β	=	reciprocal of absolute gas temperature
	=	$1/T_{amb}$
β_t	=	temporal weighting factor
β_z	=	spatial weighting factor
	=	void volume fraction
E	=	$\left(1.0 - W_t \sqrt{CD}\right)^2$
η_j^i	=	local efficiency of species i in cell j
η_{cat}^i	=	overall catalyst efficiency for species i
$\eta_{j(uniform)}^i$	=	local efficiency for species i in cell j based on $\eta_{j\ uniform}^i$ = constant for all cells
η_{map}^i	=	performance map efficiency for species i
η_{max}^i	=	maximum conversion efficiency for species i based on available oxidant
η_{red}	=	total reductant conversion efficiency
γ	=	available oxidant calculation variable

ρ_g	=	exhaust gas density (Kg/m³)
		$\dfrac{P_g Mw_g}{RT_g} = 352.55/ T_g$ (K)
ρ_w	=	wall density (Kg/m³)
$\rho_{w(cer)}$	=	density of ceramic substrate (Kg/m³)
	=	1985
$\rho_{w(Fe)}$	=	density of Iron (Kg/m³)
	=	7593
$\rho_{w(met)}$	=	density of metallic substrate (Kg/m³)
	=	8121.1
λ	=	stoichiometrically normalized air-to-fuel ratio
λ_{cat}	=	stoichiometrically normalized air-to-fuel ratio within the catalyst after adjusting for oxygen storage
λ_g	=	thermal conductivity of gas (J/m/s/K)
	=	$8.459 \times 10^{-3} + 5.7 \times 10^{-5} T_g$(K)
λ_w	=	wall thermal conductivity (J/m/s/K)
$\lambda_{w(SS)}$	=	thermal conductivity of stainless steel (J/m/s/K)
	=	$11.416 + .0130 T_w$(K)
$\lambda_{w(met)}$	=	thermal conductivity of metallic substrate (J/m/s/K)
	=	$31.0 - .0095 T_w$(K)
$\lambda_{w(Fe)}$	=	thermal conductivity of Iron (J/m/s/K)
	=	$56.653 - .01732 T_w$(K)
$\lambda_{w(cer)}$	=	thermal conductivity of ceramic substrate (J/m/s/K)
	=	$0.0506[32.734 - .01 T_w$(K)$]$
μ_g	=	dynamic viscosity of exhaust gas (N-s/m²)
	=	$[.00268 T_g$(K)$+1.384] \cdot 10^{-5}$
τ	=	thermocouple time constant (seconds)
$\chi_{O_{2store}}$	=	fractional filling of the oxygen storage capacity
ΔH_k	=	heat of reaction per mole for the kth reaction (J/g-mole)
ΔH_{CO}	=	heat of reaction for CO (J/g-mole)
	=	2.83×10^5
ΔH_{H_2}	=	heat of reaction for H_2 (J/g-mole)
	=	2.84×10^5
ΔH_{HC}	=	heat of reaction for HC (J/g-mole)
	=	6.37×10^5
Δz	=	uniform computational cell length (m)
Δz_j	=	jth computational cell length (m)